Structural Engineering and Mechanics, Vol. 6, No. 8 (1998) 883-899
DOI: http://dx.doi.org/10.12989/sem.1998.6.8.883

Stresses analyses of shell structure with large holes

Zongshu Tian† and Jinsong Liu‡

Department of Mechanics, Graduate School at Beijing, University of Science and Technology of China, Chinese Academy of Sciences, Beijing 100039, China

Abstract. The strength, deformation and buckling of a large engineering structure consisting of four ellipsoidal shells, two cylindrical shells with stiffening ribs and large holes, one conical shell and three pairs of large flanges under external pressure, self weight and heat sinks have been analysed by using two kinds of five different finite elements - four assumed displacement finite elements (shell element with curved surfaces, axisymmetric conical shell element with variable thickness, three dimensional eccentric beam element, axisymmetric solid revolutionary element) and an assumed stress hybrid element (a 3-dimensional special element developed by authors). The compatibility between different elements is enforced. The strength analyses of the top cover and the main vessel are described in the paper.

Key words: shell structure with stiffening ribs; large holes; strength analyses; finite element method.

1. Introduction

A large engineering structure is shown in Fig. 1. It is assembled by a vertical cylindrical shell (main vessel) and a horizontal cylindrical shell (auxiliary vessel). The structure consists of four ellipsoidal shells, two cylindrical shells with stiffening ribs, one conical shell and three pairs of large flanges. The shells and the stiffening ribs are made of alloy steel and carbon steel respectively.

The characteristics of this structure are as follows: 1) complicated and huge scale, two large cylindrical shells cross at 90° angle, while the conical shell and the horizontal cylindrical shell cross at 29° angle; 2) eight small circular holes, two large circular holes, a large egg-shaped hole and two rectangular holes on the shells and all of them are strengthened by stiffening plates with different widths. The scale of some large holes exceeds the allowed range given by the National Standard (Chinese Standard Press 1993); 3) submitted to external pressure, self weight, and heat sinks which are distributed along different height of the top ellipsoidal shell, vertical cylindrical shell and horizontal cylindrical shell.

The strength analyses of the structure consist of three parts (Fig. 1): 1) the top cover of the main vessel, 2) the main vessel, 3) the auxiliary vessel. The first two parts are described in this paper.

† Professor
‡ Research Assistant

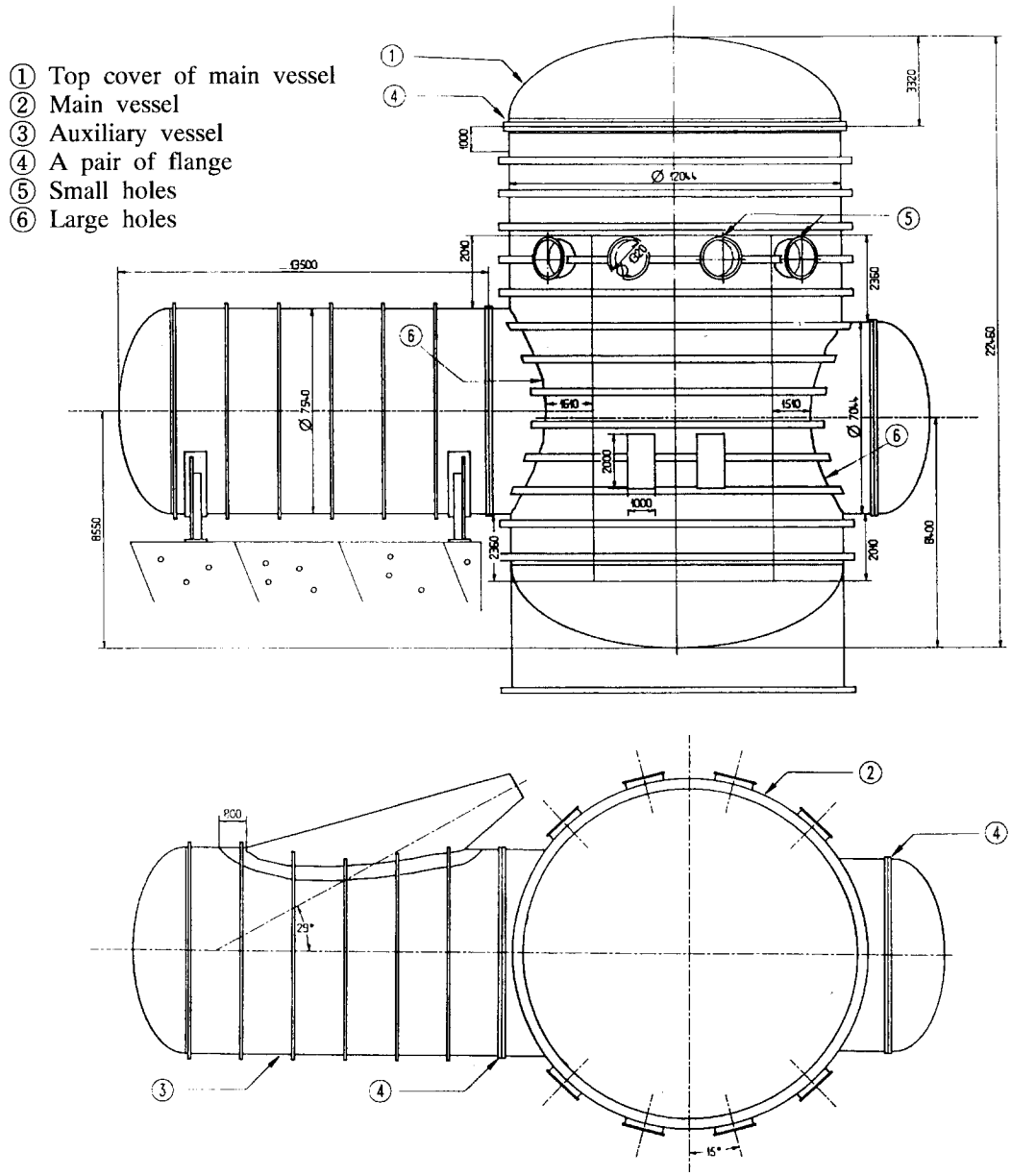

Fig. 1 Sketch of the structure

2. The numerical procedure

2.1. The computational model of strength analyses

The computational model consists of four sections: the top cover of the main vessel, left half of the main vessel and the auxiliary vessel, auxiliary vessel, and the main vessel. The model is based on following considerations:

1) Previous experimental results show that the difference in stresses obtained by the use of global calculation and separate calculation is only less than 1.5% for the strength analysis of shell with holes (Xu *et al.* 1987). The difference of stresses can reach 12% when the stiffening ribs are counted or not (Su 1989). In the present analyses, separate models are used. The ribs and its eccentricity are counted.

2) The boundaries of the sections are located far away from the local stress zones

- Numerical results show that the maximum local stress zones are approximately equal to $0.63r$ (θ=0°, θ is measured from the generatrix of shell. r: radius of hole) and $0.45r$ (θ=90°) respectively for cylindrical shells with large holes (Su 1989, Wang *et al.* 1988). Meanwhile, the experimental results show that the local stress zones are approximately equal to $0.5r$ for cylindrical shell with regular holes (Xu *et al.* 1987). Therefore, the local stress zones for the present structure are estimated as follows:
  At the left large hole ($2r$=7.5m) of the main vessel: θ=0°, $0.63r$=2.36m; and θ=90°, $0.45r$= 1.69m;
  At the right large hole ($2r$=7.0m) of the main vessel: θ=0°, $0.63r$=2.21m; and θ=90°, $0.45r$= 1.58m.
- Experimental results also point out that the zone between two rows of parallel holes in the direction of generatrix of a cylindrical shell is sensitive to the stress concentration. But it is insensitive to the stress concentration in the circumferential direction (Xu *et al.* 1987).

3) The boundaries of the sections are located far away from the local borders of boundary effect.

Theory of shells points out that the border is approximately equal to (2.0-2.5) $\sqrt{Rt}$ (R: radius of shell, t: thickness of shell, Timoshenko *et al.* 1959, Xu 1982). In the present analyses it equals to 1.1m and 0.7m apart from the upper flange and the left flange of the main vessel respectively.

4) One characteristic of the top cover of the main vessel is that the upper and lower flanges are tightened by external loads without bolts. The top cover can be considered as one section of the strength analyses.

Based on above analyses the computational model consists of four sections for strength analyses. The eccentric stiffening ribs and the stiffening plates with different widths around the holes are included.

2.2. Selection of finite element

1) Cylindrical shells and left ellipsoidal shell: 8-node shell element with curved surface and variable thickness is selected (Fig. 2, Wang *et al.* 1988, Xin *et al.* 1981). Each node has five degree-of-freedom (dof) (u_i, v_i, w_i, α_i, β_i).

Let ξ, η, ζ be local coordinates on the middle plane of shell ($-1 \leq \xi, \eta, \zeta \leq 1$) and t_i be the thickness of shell at point i. The global coordinates at arbitrary point in the shell element are given by

$$\begin{Bmatrix} x \\ y \\ z \end{Bmatrix} = \sum_{i=1}^{8} N_i(\xi, \eta) \begin{Bmatrix} x_i \\ y_i \\ z_i \end{Bmatrix}_{middle-plane} + \sum_{i=1}^{8} N_i(\xi, \eta) \frac{\zeta t_i}{2} V_{3i} \tag{1}$$

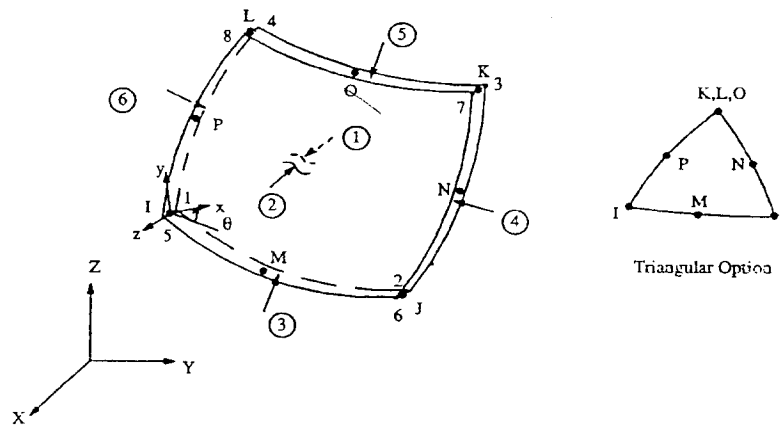

Fig. 2 8-node shell element with curved surface

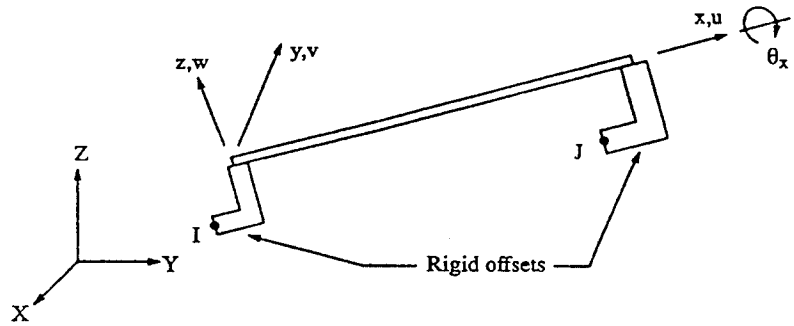

Fig. 3 2-node 3-D tapered unsymmetrical beam element

where $$V_{3i} = \begin{Bmatrix} x_i \\ y_i \\ z_i \end{Bmatrix}_{upper-plane} - \begin{Bmatrix} x_i \\ y_i \\ z_i \end{Bmatrix}_{bottom-plane} = \begin{Bmatrix} \Delta x_i \\ \Delta y_i \\ \Delta z_i \end{Bmatrix}$$

The displacements and shape functions are given by following equations:

$$\begin{Bmatrix} u \\ v \\ w \end{Bmatrix} = [N_1 \ N_2 \cdots N_8] \begin{Bmatrix} \boldsymbol{a}_1 \\ \boldsymbol{a}_2 \\ \vdots \\ \boldsymbol{a}_8 \end{Bmatrix} \tag{2}$$

where $\boldsymbol{a}_i = [u_i,\ v_i,\ w_i,\ \alpha_i,\ \beta_i]^T \qquad (i = 1, 2, \cdots 8)$

$$N_i = (1+\xi_0)\,(1+\eta_0)(\xi_0+\eta_0-1)\,\frac{\xi_i^2\eta_i^2}{4} + (1-\xi^2)(1+\eta_0)(1-\xi_i^2)\,\frac{\eta_i^2}{2}$$

$$+(1-\eta^2)(1+\xi_0)(1-\eta_i^2)\,\frac{\xi_i^2}{2} \qquad \xi_0 = \xi_i\,\xi \qquad \eta_0 = \eta_i\,\eta \tag{3}$$

$$\boldsymbol{N_i} = \begin{bmatrix} N_i & 0 & 0 & N_i\zeta\frac{t_i}{2}l_{1i} & -N_i\zeta\frac{t_i}{2}l_{2i} \\ 0 & N_i & 0 & N_i\zeta\frac{t_i}{2}m_{1i} & -N_i\zeta\frac{t_i}{2}m_{2i} \\ 0 & 0 & N_i & N_i\zeta\frac{t_i}{2}n_{1i} & -N_i\zeta\frac{t_i}{2}n_{2i} \end{bmatrix} \tag{4}$$

$$V_{1i} = \begin{Bmatrix} l_{1i} \\ m_{1i} \\ n_{1i} \end{Bmatrix} = \frac{1}{\sqrt{\Delta y_i^2 + \Delta z_i^2}} \begin{Bmatrix} 0 \\ -\Delta z_i \\ \Delta y_i \end{Bmatrix} \tag{5}$$

$$V_{2i} = \begin{Bmatrix} l_{2i} \\ m_{2i} \\ n_{2i} \end{Bmatrix} = \frac{1}{t_i\sqrt{\Delta y_i^2 + \Delta z_i^2}} \begin{Bmatrix} \Delta y_i^2 + \Delta z_i^2 \\ -\Delta x_i \Delta y_i \\ \Delta x_i \Delta z_i \end{Bmatrix} \tag{6}$$

One property of the shell element with curved surface is that it has already considered the effects of transverse shear deformation. Therefore the rotations of middle plane are independent variables which do not depend on the first order derivative of the displacement. Consequently, it only requires the continuity of the displacement function on the interelement surface and does not require the continuity of its first order derivative.

The shell element with curved surface has the following advantages:

- In comparison with the plate-shell element which consists of plane stress element and plate bending element:

  First, the error of the geometry approximation and the disturbance of the local stresses induced by the discontinuity of the tangent along the direction perpendicular to the interelement boundary can be avoided by using the shell element instead of using the plate-shell element to discretize the shell.

  Second, even though a plate-shell element is constructed by a compatible plane stress element and a compatible plate element, the plate-shell elements can still be incompatible if the interpolating functions of u, v and w are different on the interelement boundaries. On the other hand, if the same power interpolating functions of u, v, w are used, and similar to w, the first order derivatives of u, v are also included in the node parameters, it not only will greatly increase the number of degree-of-freedom of the system and the complexity of displacement formulation, but also will result in unbalanced internal forces and thus produce larger errors when the thicknesses of the neighbouring elements are different. It is quite unfavourable to the stresses analyses nearby large holes strengthened by stiffening plate in present structure. All these problems can be avoided by the use of the shell element with curved surface.

  Meanwhile, since the membrane strains have been coupled with normal displacement effect, the shell element can better simulate the real state especially at boundary zone induced by the discontinuity of the structure or loads - this is the point that the present strength

analyses must pay special attention to.

- In comparison with flat shell element
  Numerical examples show that although flat shell elements make some improvements in comparison with plate-shell elements, both results are very close. The strain-displacement relation of flat shell is obtained under the approximate conditions of $(\partial z/\partial x)^2 \ll 1$ and $(\partial z/\partial x)^2 \ll 1$. It can not ensure that the strain will not be raised under the condition of rigid body movements. The present shell element ensures the necessary rigid body mode and the convergence condition. Its accuracy is higher than those of flat shell elements.
- The shell element with variable thickness is also applicable when it is degenerated into triangle. So, the shells of the structure are easily discretized by the use of this shell element specially in the zone near the holes.
  Based on above discussion the 8-node general curved shell element with variable thickness has been used in the present analyses.

There are also some disadvantages for the shell elements: first, a great deal of computation; second, there might be shear locking for thin shell wherein a reduced integration method has been used to avoid the problem.

2) Stiffening ribs: 2-node, 3-D tapered unsymmetrical beam elements (Fig. 3, each node with 6 dof - u, v, w, θ_x, θ_y, θ_z).

The element represents the real working situation of the stiffening ribs on the outer surface of the main and auxiliary vessel. Its element stiffness matrix can easily be assembled with other element stiffness matrices.

3) Top ellipsoidal shell and the neck of upper flange: 2-node axisymmetric conical shell elements with variable thickness (Fig. 4, each node with 4 dof - u, v, w, θ_z).

4) Ring of upper flange: 4-node axisymmetric revolutionary solid elements (each node with 3 dof - u, v, w).

5) Along the rim of small holes (Fig. 1): 8-node 3-dimensional special assumed stress hybrid elements (Fig. 5, Tian *et al.* 1990). It can provide more accurate stresses along the rim of hole than those obtained by using ordinary assumed displacement elements and ordinary assumed stress elements.

The constraint equations of the displacement on the interelement surfaces of the five different kinds of elements are established to ensure the compatibility.

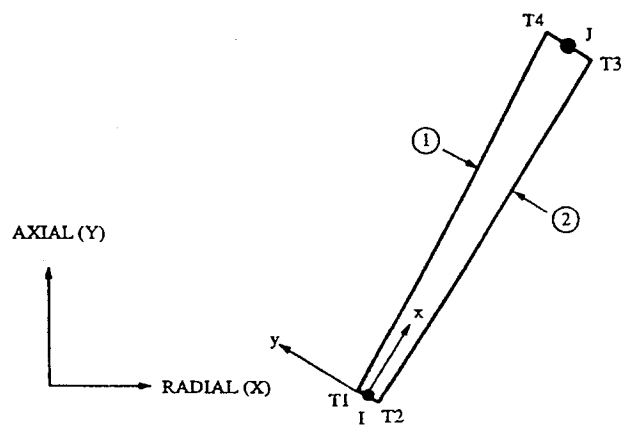

Fig. 4 2-node axisymmetric conical shell elements

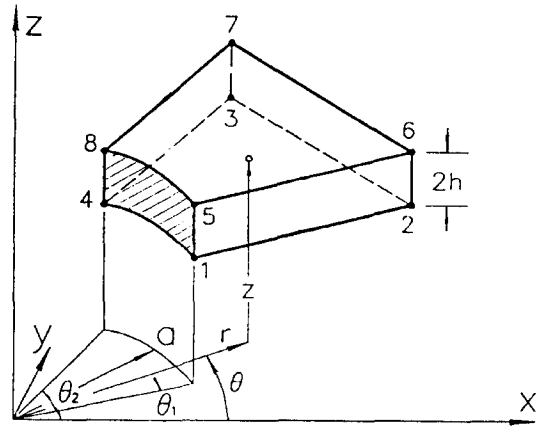

Fig. 5 8-node 3-D special assumed stress hybrid elements

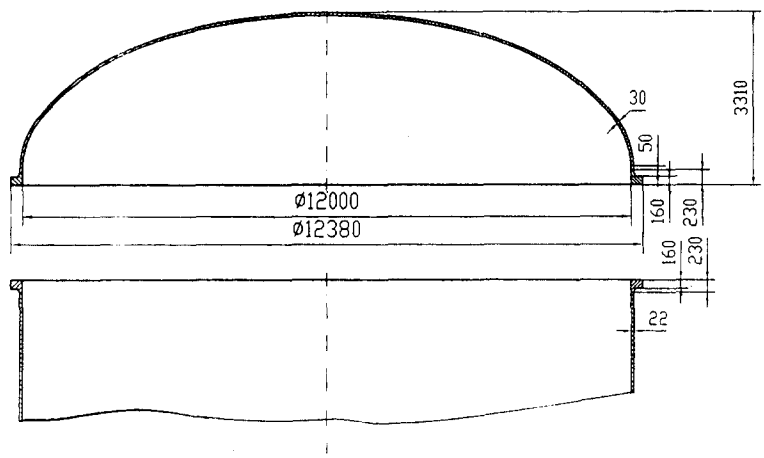

Fig. 6 Top cover of the main vessel

3. Computation of top cover of the main vessel

The structure of the top cover is shown in Fig. 6. It consists of an ellipsoidal shell, a pair of large flanges and a rubber spacer between the two large flanges (Fig. 7). The first step of strength analyses of the assembled shell structure is the computation of top cover. Since the computed forces and moments are transferred directly to the main shell, the analytical accuracy of the top cover will directly affect the accuracy of the main vessel.

There are two characteristics of the top cover: 1) The flanges are very large. 2) The upper and lower flanges are tightened by external pressure and self weight without bolts.

The calculation of regular flange usually is based on Waters method (Timoshenko *et al.* 1959, Ding 1992) wherein the simple strength design is used instead of equivalent calculation of seal design. The hermetic seal and safety of the whole connection design are ensured by the sufficient stiffness of the flange controlled by so called "elastic stress". It should be noted that the following approximate assumptions are used in the method: 1) The external pressure is neglected. 2) The radial displacement at the large end of neck cone equals to zero, but

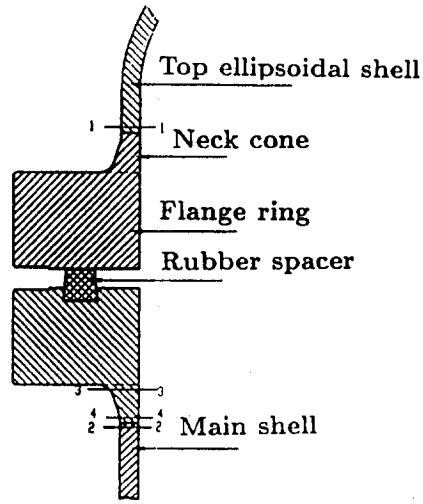

Fig. 7 Connection of top cover and flanges

there is a rotation at the ring of flange. In fact, these assumptions will result in incompatibility at the junction of neck cone and flange ring and serious errors for large scale flange (diameter $\geq$ 1.5m).

The Murray-Stuart method for analysing flange simplifies the neck cone as a cylindrical shell with variable thickness and the ring of flange as a ring with certain thickness (Fan 1979, Murray *et al.* 1961). It makes some improvement compared to the above method. But the method is based on the assumption of geometric shape that the radius of cylindrical shell connected with the flange is the average radius of neck cone and ring of the flange. And it also leads to errors for flange.

In the paper both of the above assumptions are abandoned. Three computational schemes are proposed and compared in order to approach to real working state of the large scale flange. The strength checks of the flange and top ellipsoidal shell have been done.

3.1. The computational schemes of top cover

The following three kinds of schemes were proposed (Table 1) and the results were

Table 1 Computational schemes of the top cover

	Flange		Ellipsoidal shell	Relation of displacement
	Neck cone	Ring		
1	Axisymmetric conical shell with variable thickness	revolutionary solid	Axisymmetric shell	Compatible generalized displacements at connection places of neck ring and ellipsoidal shell
2	Whole flange as a revolutionary solid		Axisymmetric shell	Compatible displacements between neck cone and ellipsoidal shell
3	Neck cone and ring as a rigid body		Axisymmetric shell	Clamping connection between cone and ellipsoidal shell

Table 2 Types of finite element and computational DOF in the top cover

Scheme	No. of element	Types of finite element	DOF
		Flange	
1	570	Axisymmetric shell element +axisymmetric solid element	-
2	656	axisymmetric solid element	-
3	-		-
		ellipsoidal shell	
1	288	axisymmetric solid element	2109
2	288	axisymmetric solid element	2295
3	78	axisymmetric solid element	312

compared.

The computational scheme 1 is proposed as follows: 1) The neck cone of the large flange is regarded as axisymmetric conical shell with variable thickness. 2) The ring of the flange is treated as a revolutionary solid. 3) The ellipsoid is an axisymmetric ellipsoidal shell. The advantage of the scheme is that it not only avoids the discontinuity of radial displacement between neck cone and ring of flange in Waters method and includes external pressure, but it also avoids the assumption of geometric shape in Murray-Stuart method. Obviously, this scheme can provide more accurate results. The friction between ring and rubber spacer with 4 kinds of sliding friction factors (ν=0.00, 0.10, 0.12, and 0.15) is also counted in the scheme.

Scheme 2 regards the ring and neck cone as a whole elastomer which is simpler than Scheme 1. Scheme 3 considers the whole flange as a rigid body. It is the simplest one.

The types of finite element and the total degree-of-freedom (DOF) of each scheme are given in Table 2.

3.2. Numerical results of the top cover

1) Computed stress resultants transferred to the upper edge of the cylindrical shell

The meridian, parallel and normal line of ellipsoidal shell middle plane were defined as coordinates α, β, γ respectively (Fig. 8).

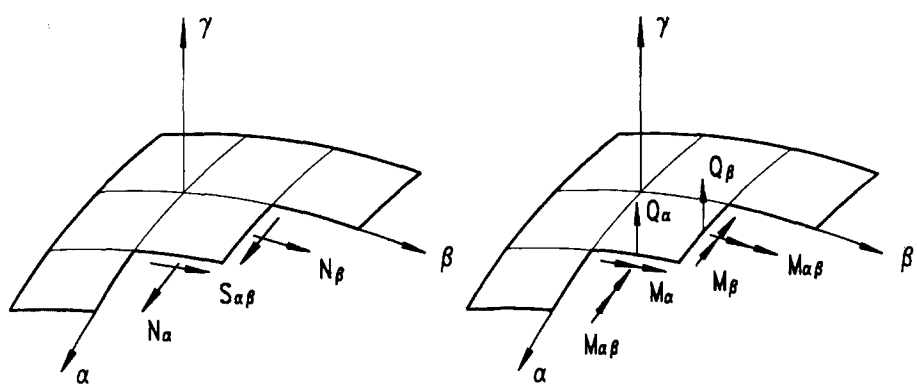

Fig. 8 Positive forces and moments of shell

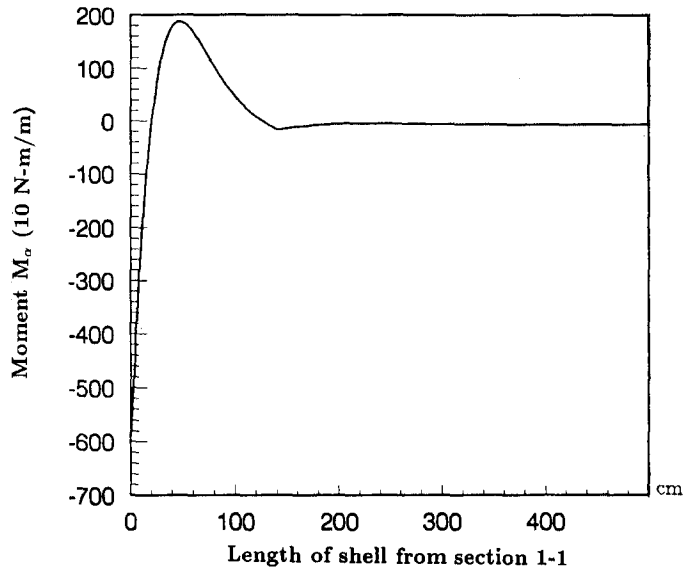

Fig. 9 Variation of M_α along meridian α of middle plane of ellipsoidal shell

Table 3 Stress resultants transferred to the cylindrical shell (ν=0.15) (ν: sliding friction factor; Fig. 7, 2-2 section)

Scheme		N_α 10^3 N/m	M_α 10^3 N-m/m	Q_α 10^3 N/m	N_β 10^3 N/m	M_β 10^3 N-m/m
1	ν=0.15	-298.76	-8.18	30.14	-657.83	-2.46
	ν=0.12	-298.82	-7.85	29.98	-660.83	-2.36
	ν=0.10	-298.86	-7.63	29.22	-661.97	-2.29
	ν=0.00	-298.81	-6.52	25.44	-672.79	-2.09
2		-297.42	-7.74	30.08	-726.56	-2.23
3		-319.92	-8.10	21.00		

Table 4 Computed stresses of dangerous section 1-1 in the ellipsoidal shell

Direction	N_α, N_β 10^3 N/m	M_α, M_β 10^3 N-m/m	Q_α, Q_β 10^3 N/m	σ^{max}, σ^{min} MPa
α	-311.45	-5.93	-33.80	σ_α^{min}=-54.46(outside of shell) σ_α^{max}=+32.88(inside of shell)
β	-240.25	-1.78	0.00	σ_β^{min}=-21.58(outside of shell) σ_β^{max}=+4.72 (inside of shell)
Strength Check	Maximum stress: σ^{max}=-54.68 MPa < $[\sigma]$=133 MPa Equivalent stress: σ_1-σ_3=87.56 MPa < $[\sigma]$			

The computed forces and moments transferred from the top cover to the cylindrical shell are given in Table 3. It is seen that the results obtained by three schemes are very close. Since the stress resultants given by ν=0.15 of scheme 1 are generally a little bit great, they are chosen in the following computation.

Table 5 The meshes of the main vesse

Mesh No.	Structure	Elements No.	DOF
1	Auxiliary vessel +1/2 main vessel	1250	12908
2	1/2 main vessel without top ellipsoidal shell	2440	29333
3	1/4 main vessel without top ellipsoidal shell	2703	37334

2) The results of the ellipsoidal shell

The computed stresses on the dangerous section 1-1 are given in Table 4.

The strength of the ellipsoidal shell is satisfied. The variation of moment M_α along meridian α of middle plane of the ellipsoidal shell is shown in Fig. 9. It is of interest to note that the local border is approximately equal to 125cm which is close to the estimated value 110cm based on shell theory (Xu 1982).

3) The numerical results of the flange

The computed results show that the strength of the flange is safe. It is also shown that the computed stresses in the large scale flange are much greater than those obtained by Waters method (Su 1989) and the maximum, the minimum stresses obtained by present method are bending stresses acting at small end of neck cone which are neglected by Waters method.

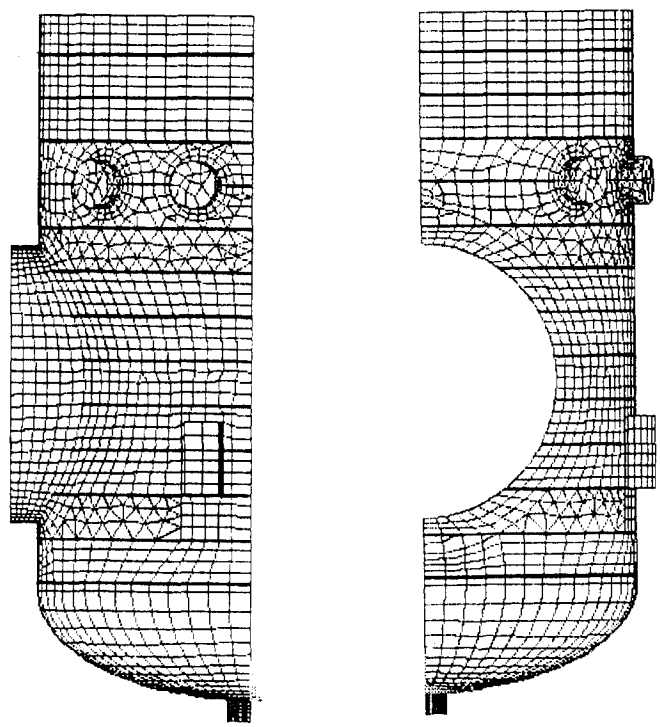

(a) Front view **(b) Side view**

Fig. 10 Mesh 3 of the main vessel

3.3. Discussion of computed results of the top cover

The numerical results show that the strength of the ellipsoidal shell and the flange is safe. The results also provide the stress resultants which are transferred to the cylindrical shell.

The present computational scheme of the large scale flange can avoid the approximate assumptions in Waters and Murray-Stuart methods, and provides more accurate stresses analyses which will not only ensure safety of the large scale flange but also will bring notable economical benefit, since price of the flange will be an important part in the whole structure.

4. Computation of the main vessel

The strength analyses of the main vessel consist of two parts: First, the auxiliary vessel and the left part of the main vessel (without top cover) are analyzed as a whole. Second, the main and the auxiliary vessels are divided at the flange (Fig. 1). The consistency of the generalized displacements between the main vessel and the auxiliary vessel is ensured. The main vessel has been computed by using submodel method (Lunkings *et al.* 1984) until the reasonably accurate results are obtained. Therefore three different meshes are used (Table 5). The mesh 3 is shown in Fig. 10.

4.1. Boundary conditions

1) At the flange connecting the auxiliary vessel to the main vessel: the generalized displacements obtained by the coarse mesh are used as the boundary conditions for the next mesh.

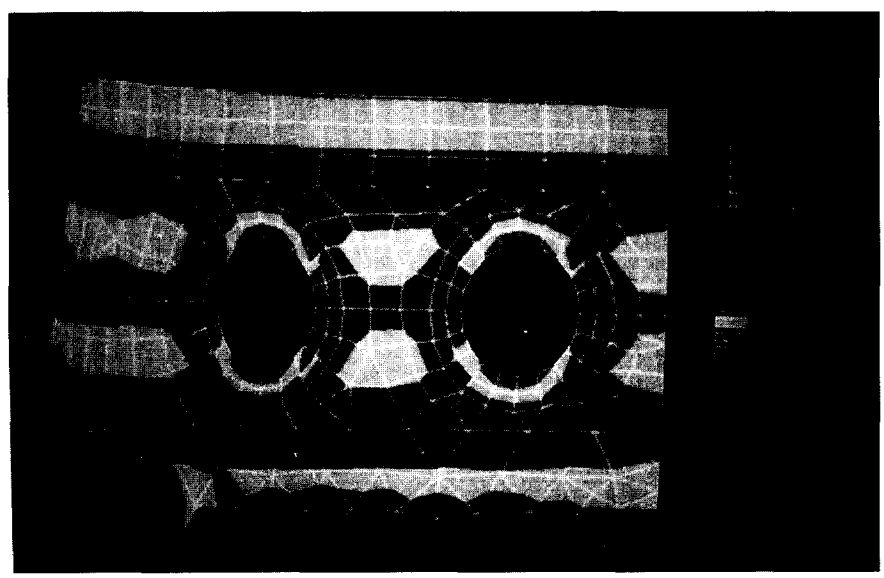

Fig. 11 The distribution of σ_θ along the top small circular holes (outer-surface)

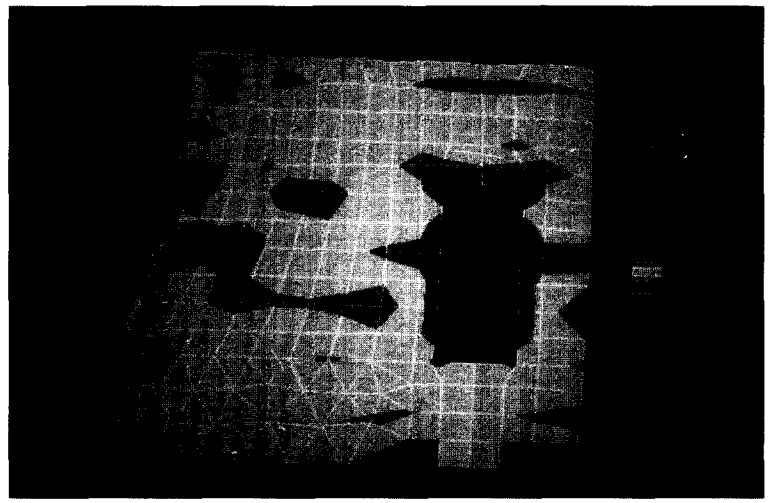

Fig. 12 The distribution of σ_θ along the rectangular hole (outer-surface)

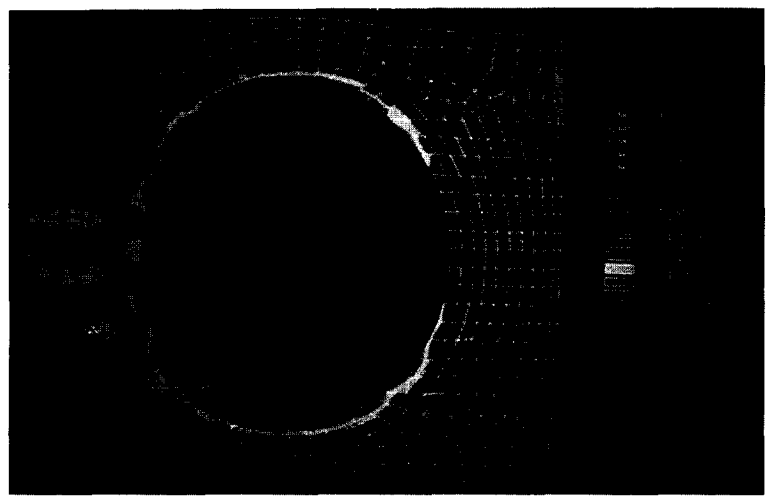

Fig. 13 The distribution of σ_θ along the left large circular hole (outer-surface)

2) At the flange connecting the top cover to the main vessel: the computed stress resultants are considered as boundary conditions.

3) At the bottom of the main vessel: completely built in.

4.2. Computed stresses of the main vessel

1) The circumferential stresses of the cylindrical shell

The computed circumferential stresses σ_θ on outer-, inner- and middle-surface of the main shell are given in Table 6 where θ is the angle from the frontal horizontal of main shell (counterclockwise direction of θ is positive). The distributions of σ_θ along the small circular holes, rectangular hole and left large circular hole are shown in Figs. 11, 12 and 13 respectively.

Table 6 The circumferential stresses σ_θ of the main vessel (MPa) (working stress [σ]=133MPa)

Location		Outer surface	Inner surface	Middle surface
Along the rim of left large circular hole	0°	22.6	41.3	32.0
	90°	-89.9	**-137.2**	-113.5
	θ=180°	-73.2	67.6	-5.5
	200°	-105.3	120.2	7.4
	245°	**-265.2**	-116.2	**-190.7**
	270°	**-201.3**	-89.9	**145.6**
Along the rim of small circular hole	0°	9.3	17.8	13.6
	θ=90°	-80.6	-41.4	-61.1
	180°	9.3	17.8	13.6
Along the rim of rectangular hole	Midpoint of long side	21.4	-7.5	6.9
	45° point	**-182.3**	6.6	87.8
	Midpoint of short side	-54.6	-64.2	59.2
Shell	σ_θ^{max}	3.2	-15.2	-5.9
	σ_θ^{min}	-32.1	-27.6	-29.9
Support	σ_θ^{max}	9.1	-11.1	-1.0

Table 7 The axial stresses σ_α of the main vessel (MPa) ([σ]=133MPa)

Location		Outer surface	Inner surface	Middle surface
Along the rim of left large circular hole	0°	-39.23	-45.7	-42.4
	90°	-112.68	**139.8**	13.6
	θ=180°	-39.23	47.0	3.9
	225°	**-259.68**	47.0	-106.3
	250°	**-186.13**	**139.2**	-23.4
	270°	**-186.13**	**170.7**	-7.7
Along the rim of small circular hole	0°	-24.52	-25.5	-25.0
	θ=90°	-59.43	48.2	-5.5
	180°	-24.52	-25.5	-25.0
Along the rim of rectangular hole	Midpoint of long side	23.73	-35.3	-5.7
	45° point	**-155.44**	74.4	-40.5
	Midpoint of short side	23.73	37.8	30.7
Shell	σ_α^{max}	24.81	-46.7	-10.9
	σ_α^{min}	-34.72	6.9	-13.9
Support	σ_α^{max}	17.65	-51.1	-16.7

It can be seen from the results:

- In the zone of back half of left large hole (θ=90°~270°, especially in the region of lower 1/4 part of the hole i.e., θ=180°~270°) the local circumferential stresses σ_θ at some points on outer-, inner- and middle-surface are still very large even though the hole is strengthened by stiffening plates.
- The stress concentration factor of σ_θ can be up to 9.7. But the peak stresses are limited to a very narrow region. When θ=90°, the decay border is about equal to 180cm which is very close to the estimated value (169cm).

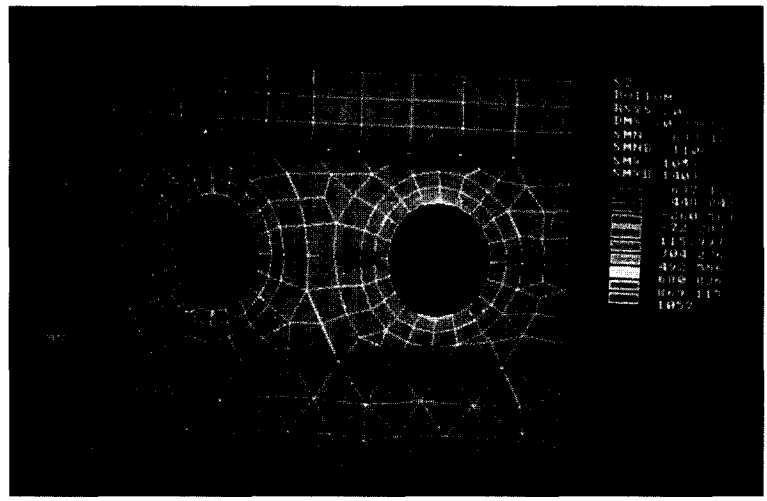

Fig. 14 The distribution of σ_α along the small circular holes (inner-surface)

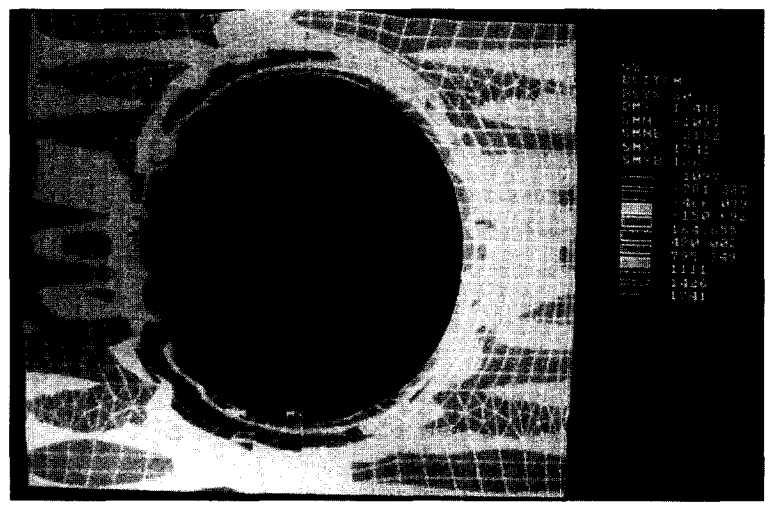

Fig. 15 The distribution of σ_α along the left large circular hole (inner-surface)

- The stresses will decrease greatly if the rectangular hole is rounded at 45°.

2) The axial stresses of the main shell

The computed axial stresses σ_α are given in Table 7. The distributions of σ_α along the small circular holes and the left large hole are shown in Figs. 14 and 15 respectively.

The results show that:

- It is similar to σ_θ that in the zone of back half of left large hole the local axial stresses σ_α on outer- and inner-surface are very great. The maximum compression stress and the maximum tension stress can reach to 2 and 1.3 times working stress respectively.
- When θ=225°~275°, since the auxiliary vessel is connected to the main vessel, it produces high local bending stress. The axial bending stresses σ_α reach $\pm$154~$\pm$179 MPa (working stress $[\sigma]$=133MPa). The stresses are higher than the circumferential bending stresses.
- Along the rim of left large hole the computed σ_α and σ_θ on the inner- and outer-surface of

Table 8 The difference of principal stresses $\sigma_1 - \sigma_3$ of the main vessel (MPa) (working stress $[\sigma]$= 133MPa)

Location		Outer surface	Inner surface	Middle surface
Along the rim of left large circular hole	0°	39.23	41.0	40.5
	90°	130.72	**202.9**	**166.9**
	θ=180°	100.22	65.0	82.6
	220°	**283.32**	**338.2**	**311.2**
	250°	**252.72**	**332.8**	**287.8**
	270°	**222.22**	**273.1**	**247.7**
Along the rim of small circular hole	0°	41.81	27.4	34.7
	θ=90°	76.39	97.4	86.9
	180°	41.87	27.4	34.7
Along the rim of rectangular hole	Midpoint of long side	54.82	52.1	53.5
	45° point	**133.27**	99.2	117.9
	Midpoint of short	82.08	114.5	95.7
Shell		100.22	96.2	98.2

the shell are close to each other, but on the middle-surface the $\sigma_\theta^{max} \geq \sigma_\alpha^{max}$.

- The circumferential stresses σ_θ and the axial stresses σ_α in the region far away from the hole are close to the theoretical results for cylindrical shell with stiffening ribs under uniform external pressure (Kalotkin *et al.* 1958).

3) The difference of principal stresses $\sigma_1 - \sigma_3$ of the main shell

The difference of principal stresses $\sigma_1 - \sigma_3$ is given in Table 8.

It can be seen from the results that the difference of principal stresses $\sigma_1 - \sigma_3$ at some points of back half of the left large hole θ=180°~270°) on outer-, inner- and middle-surface can reach to 2.5$[\sigma]$. At the top of the hole θ=90° it is 1.5$[\sigma]$. The local stresses are also distributed in a narrow region.

4) The computed stresses of stiffening ribs of the main shell

All of the maximum stresses in the stiffening ribs are smaller than the working stress $[\sigma]$ of rib.

4.3. Discussion of computational results of the main vessel

The stresses σ_θ, σ_α and $\sigma_1 - \sigma_3$ at some points of the left large hole are greater than the working stress. The maximum axial bending stress is greater than the maximum circumferential bending stress and also greater than the working stress.

For the cylindrical shell with large hole although the hole is strengthened by stiffening plate with equal area method, there still exist very high local stresses.

All the stresses along the rims of small hole, in the rest area of the shell, in the circumferential support at the bottom and in the stiffening rings are less than working stresses besides the stresses at the corner of the rectangular hole which has to be rounded.

5. Conclusions

A reasonable computational model has been proposed based on theory of shell, experiment

reports of shell with holes, numerical results of shell with large holes and the characteristics of the structure. Two kinds of five different finite elements – four assumed displacement elements and an assumed stress finite element – with favourable feature are chosen. The compatibility between different elements is ensured by established constraint equations. An advanced code is used for the strength analysis of the large complicated shell structure. The engineering design has been revised based on the computational results. The structure was constructed in 1997.

References

Ding, B.M. (1992), *Steel Pressure-Vessel – Design, Manufacture and Inspection*, Haudaong Chemistry Institute Press, Shanghai.

Fan, Q.S. (1979), *Stress Analysis and Strength Design of Pressure-Vessel*, Atomic-Energy Press, Beijing.

Kalotkin *et al.* (1958), *Bending and Stability of Plate and Cylindrical Shell*, Chinese version, Education Press, Beijing.

Lunkings, W.M., Hoa, S.V. and Sanker, T.S. (1984), "The effect of geometry of interlaminar stresses of $[0/90]_s$ composite laminates with circular holes", *J. Comp. Mat.*, **18**, 188-198.

Murray, N.W. and Stuart, D.G. (1961), "Behaviour of large taper hub flanges", *Proc. Sump. Pressure Vessel Research Towards Better Design.*

Su, W. (1989), "The design of main vessel and its analysis by using finite element method", M.S. Thesis, Chinese Academy of Space Technology.

The 3nd Editorial Office of Chinese Standard Press (1993), *A Corpus of National Standard of Pressure Vessel* (1992), Chinese Standard Press, Beijing.

Tian, Z.S. and Yuan, K.M. (1990), "Hybrid solid element with a uniform-loading cylindrical surface", *J. Comput. Struc. Mech. Appl.*, **7**, 105-108.

Timoshenko, S.P. and Woinowsky-Krieger, S. (1959), *Theory of Plates and Shells*, McGraw-Hill Book Company, New York.

Wang, X.C. and Shao, M. (1988), *The Foundations of Finite Element Methods and Numerical Methods*, Tsinghua University Press, Beijing.

Wang, X.H. and Su, W. (1988), "The analysis of structure with large holes by using finite element method", Research Report, Chinese Academy of Space Technology, HT-880599.

Xin, Y.Q. and He, F.B. (1981), *The Finite Element Method in Elasticity and Plasticity*, Mech. Indus. Press, Beijing.

Xu, B.H., Pei, J.H. and Zhu, B.J. (1987), *The Theory and Experiment of Shell with Holes*, National Defence Indus. Press, Beijing.

Xu, Z.L. (1982), *Theory of Elasticity*, **2**, 2nd eds, Education Press, Beijing.